\



Tunable terahertz transmission behaviors and coupling mechanism in hybrid MoS_2 metamaterials

Yuwang Deng(邓雨旺), Qingli Zhou(周庆莉)†, Wanlin Liang(梁菀琳), Pujing Zhang(张朴婧), and Cunlin Zhang(张存林)

Citation: Chin. Phys. B, 2022, 31 (**1**): 014101. DOI: 10.1088/1674-1056/ac1fde
Journal homepage: http://cpb.iphy.ac.cn; http://iopscience.iop.org/cpb

What follows is a list of articles you may be interested in

High-confinement ultra-wideband bandpass filter using compact folded slotline spoof surface plasmon polaritons

Xue-Wei Zhang(张雪伟), Shao-Bin Liu(刘少斌), Ling-Ling Wang(王玲玲), Qi-Ming Yu (余奇明), Jian-Lou(娄健), and Shi-Ning Sun(孙世宁)
Chin. Phys. B, 2022, 31 (**1**): 014102. DOI: 10.1088/1674-1056/ac22a2

A novel receiver-transmitter metasurface for a high-aperture-efficiency Fabry-Perot resonator antenna

Peng Xie(谢鹏), Guangming Wang(王光明), Binfeng Zong(宗彬锋), and Xiaojun Zou(邹晓鋆)
Chin. Phys. B, 2021, 30 (**8**): 084103. DOI: 10.1088/1674-1056/ac0788

Shared aperture metasurface antenna for electromagnetic vortices generation with different topological charges

He Wang(王贺), Yong-Feng Li(李勇峰), and Shao-Bo Qu(屈绍波)
Chin. Phys. B, 2021, 30 (**8**): 084101. DOI: 10.1088/1674-1056/abe37c

Characteristic mode analysis of wideband high-gain and low-profile metasurface antenna

Kun Gao(高坤), Xiang-Yu Cao(曹祥玉), Jun Gao(高军), Huan-Huan Yang(杨欢欢), and Jiang-Feng Han(韩江枫)
Chin. Phys. B, 2021, 30 (**6**): 064101. DOI: 10.1088/1674-1056/abdb23

Design and verification of a broadband highly-efficient plasmonic circulator

Jianfei Han(韩建飞), Shu Zhen(甄姝), Weihua Wang(王伟华), Kui Han(韩奎), Haipeng Li(李海鹏), Lei Zhao(赵雷), and Xiaopeng Shen(沈晓鹏)
Chin. Phys. B, 2021, 30 (**3**): 034102. DOI: 10.1088/1674-1056/abca23

Tunable terahertz transmission behaviors and coupling mechanism in hybrid MoS_2 metamaterials

Yuwang Deng(邓雨旺), Qingli Zhou(周庆莉)†, Wanlin Liang(梁菀琳), Pujing Zhang(张朴婧), and Cunlin Zhang(张存林)

Key Laboratory of Terahertz Optoelectronics, Ministry of Education, and Beijing Advanced Innovation Center for Imaging Theory and Technology, Department of Physics, Capital Normal University, Beijing 100048, *China*

(Received 14 July 2021; revised manuscript received 16 August 2021; accepted manuscript online 22 August 2021)

A hybrid metamaterial with the integration of molybdenum disulfide (MoS_2) overlayer is proposed to manipulate the terahertz (THz) wave. The simulated results indicate that the introduction of MoS_2 layer could significantly modify the resonant responses with large resonance red-shift and bandwidth broadening due to the depolarization field effect, especially for the structure on the small permitivity substrate. Additionally, the wide-band modulator in off-resonant region and a switch effect at resonance can be achieved by varying the conductivity of MoS_2 layer. Further theoretical calculations based on the Lorentz coupling model are consistent with the simulated results, explicating the response behaviors originate from the coupling between MoS_2 overlayer and the metastructure. Our results could provide a possibility for active control THz modulator and switchable device based on the MoS_2 overlayer and advance the understanding of the coupling mechanism in hybrid structures.

Keywords: terahertz metamaterial, MoS_2, coupling mechanism, switchable device

PACS: 41.20.Jb, 42.15.Eq, 42.25.Bs, 42.25.Dd **DOI:** 10.1088/1674-1056/ac1fde

1. Introduction

The transition metal dichalcogenides have earned extensive attention in recent years due to the potential application for novel semiconductor devices. This family of compounds displays abundant electronic properties ranging from semiconductor, semimetal, metal, and even to superconductor depending on the choice of transition metal,[1] one of which is MoS_2 with outstanding optical and electronic properties.[2–4] The bulk MoS_2 crystal is an indirect bandgap semiconductor but it can be transformed into a direct semiconductor in the monolayer limit, which makes it attractive for photoluminescent applications.[5] After the established synthesis and fabrication strategies, MoS_2 has been employed in field effect transistors,[6] integrated circuits,[7] optoelectronic devices,[8,9] light generation and harvesting,[10–13] valleytronics,[14] van der Waals heterostructures,[15,16] and mimic synaptics.[17]

Metamaterials are the artificially structured composite arrays of subwavelength structures. Their extraordinary physical properties cannot be obtained in natural materials, such as negative refractive index,[18,19] sub-diffraction imaging,[2] perfect absorption,[21] and electromagnetic cloaking.[22,23] Those special properties originate from electromagnetic interaction between incident radiation and those man-made structures.[24–26] Especially, the MoS_2-metamaterial integrated devices have been exploited to manipulate electromagnetic resonant behaviors combined with the excellent properties of MoS_2 layer and the novel functionalities of metamaterials.[9,27] Such hybrid structures with optically controlled conductivity of MoS_2 can realize tunable sharp Fano resonances and tailored plasmon-induced transparency in the THz range. Few studies have been carried out to explore the influence of MoS_2 on other resonance modes, as well as the coupling mechanism between MoS_2 layer and metamaterial. Split ring resonantor (SRR) as a classical metamaterial structure, which has both electrical and magnetic responses with two different resonance modes defined as inductance–capacitance (LC) resonance and dipole resonance,[28,29] has become the basic building block for intensive research of THz metamaterials and other hybrid metaphotonic devices. Those studies have successfully illustrated the manipulation of slow light,[30] ultrafast all-optical switch,[31] dynamical resonance frequency shift,[32] and controllable all-optical modulation speed.[33,34] It is obvious that the SRR is a fundamental and important structural unit to further develop and expand the THz device functions.

Here, we have proposed the hybrid MoS_2/SRR structures to investigate the overlayer induced change and optical control in transmission spectra from the simulated and theoretical calculations. Compared with the other two substrates, we have found the remarkable change with large red-shift at resonant frequencies and broad bandpass in non-resonant region after covering the MoS_2 layer onto SRR with SiO_2 substrate. The simulated results have proved the introduction of MoS_2 could significantly engineer the transmitted spectra due to depolarization field effect verified by the simulated electric field distributions. In addition, a 38% broad band modulation from 0.95 THz to 1.95 THz and 100% modulation of the resonances

†Corresponding author. E-mail: qlzhou@cnu.edu.cn

© 2022 Chinese Physical Society and IOP Publishing Ltd

with a switchable effect can be achieved via tuning conductivity of the MoS_2 overlayer. It is worth noting that the LC resonance is more easily tailored than the dipole resonance with the varied conductivity of MoS_2. We have further utilized the coupled Lorentz oscillator model to theoretically calculate the influence of MoS_2 on the THz response spectra accompanied with resonance red-shift, bandwidth broadening, and intensity change, which originate from the coupling and damping between MoS_2 overlayer and SRR structure. Our results imply that the conductivity-engineered switchable device and controllable broad band THz modulator could be implemented through hybrid MoS_2 metastructures.

2. Simulated results and theoretical discussion

For exploring the resonant behaviors of our proposed hybrid MoS_2 metamaterial, numerical calculations are performed based on the finite integration method with the periodic boundary conditions. The schematic structure and the unit cell of the hybrid MoS_2/SRR structure are depicted in Fig. 1 with three layers including MoS_2 layer, gold arrays, and substrate. In our simulation, the thickness of Au is 200 nm and the substrate is 250 μm. A MoS_2layer with the thickness of 400 nm is covered on SRR structure surface. The periodic length is 50 μm in both x and y directions. The THz wave polarizing along x axis is normally incident to the structure surface, as shown in Fig. 1(a). Here, GaAs, Si, and SiO_2 with dielectric constants of 12.9, 11.56, and 3.75, respectively, are used as substrates, and Au (lossy metal) with conductivity of 3.56×10^7 S/m is considered to form the metallic SRR array. The permittivity of MoS_2 is set to be 12.25.[9]

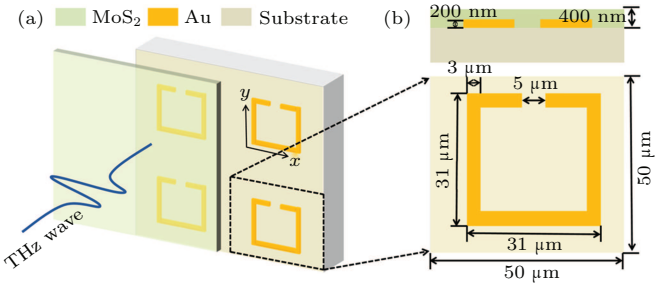


Fig. 1. (a) Illustration of the MoS_2/SRR structure with incident THz wave. (b) The schematic diagram of unit cell of the SRR highlighting the structural dimensions. The top-right insert is the cross-section of the unit cell.

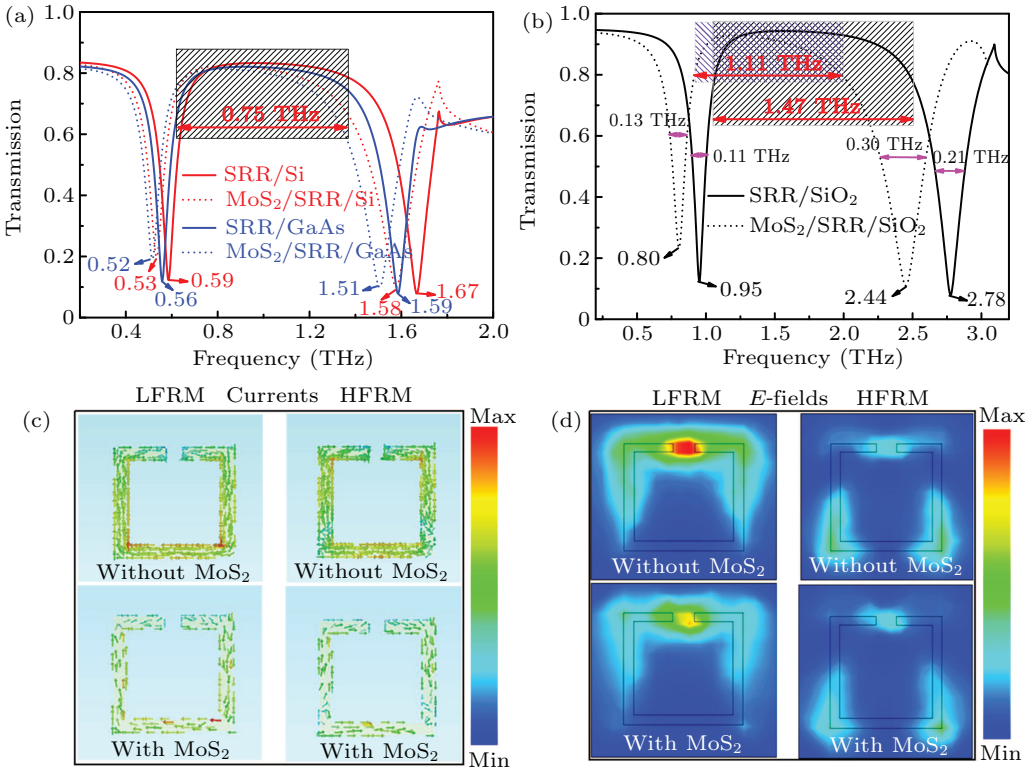


Fig. 2. THz transmission of SRR and MoS_2/SRR hybrid structures on semiconductor (a) and SiO_2 (b) substrates, respectively. The simulated surface currents (c) and electric field distributions (d) of SRR/SiO_2 without and with MoS_2 overlayer at LFRM and HFRM.

As plotted in Fig. 2(a), when the polarization of the incident THz wave is parallel to the gap-bearing side of SRR, the THz transmission responses of SRR without and with MoS_2 exhibit remarkable spectral variations. The transmission spectra of SRR structure on Si and GaAs substrates reveal two resonant responses, corresponding to low frequency resonant mode (LFRM) at ∼ 0.59 (Si substrate) and ∼ 0.56 THz (GaAs substrate), and high frequency resonant mode (HFRM) at ∼ 1.67 (Si substrate) and ∼ 1.58 THz (GaAs substrate), respectively. In addition, there is a broad transmission window of 0.75 THz in non-resonant region lying between the above two resonances. When the SRR metamaterials are covered

with MoS_2, the spectral responses can be modulated significantly. The transmission of LFRM and HFRM is slightly increased in resonant region and decreased in off-resonant region. The red-shift frequencies of LFRM and HFRM are also clearly and quantitatively recorded in Table 1. It is evident that the optical properties of metastructures on Si and GaAs substrates are similar in the THz region.

Then we further choose SiO_2 substrate, which has a large difference in dielectric constant compared with the above two substrates, to study the influence of the dielectric environment on the SRR arrays. The simulated results are presented in Fig. 2(b) for the SRR/SiO_2 structure. Without and with the introduction of MoS_2 overlayer, the THz transmission variation and resonant frequency shift of LFRM and HFRM are illustrated in Table 1. Additionally, a broadening of resonant lineshape can be observed, corresponding to values of full width at half maximum (FWHM) from 0.11 THz to 0.13 THz for LFRM, and 0.21 THz to 0.30 THz for HFRM, respectively. In the off-resonant regions, as shown in the black shadow, the bandwidth of the transmission window is much broader than that in Fig. 2(a), showing 1.47 THz without overlayer and 1.11 THz with MoS_2, respectively. Based on the above observations, it can be concluded that the THz response variation of SRR/SiO_2 without and with MoS_2 overlayer is more sensitive than those on Si and GaAs substrates, accompanied with large transmission change and frequency red-shift in resonant region, and wider transmission bandwidth in off-resonant region. Our obtained results also indicate the overlayer material has the ability to tune the THz spectral responses via changing the surrounding dielectric environments.

Table 1. THz transmission and resonant frequency shift of LFRM and HFRM without and with MoS_2 overlayer.

Substrate	T_{LFRM} SRR (%)	T_{LFRM} MoS_2-SRR (%)	ΔT_{LFRM} (%)	Δf_{LFRM} (THz)	T_{HFRM} SRR (%)	T_{HFRM} MoS_2-SRR (%)	ΔT_{HFRM} (%)	Δf_{HFRM} (THz)
Si	12.26	19.82	7.56	0.06	7.91	9.95	2.04	0.09
GaAs	12.07	19.11	7.04	0.04	7.79	9.84	2.05	0.08
SiO_2	12.29	23.43	10.53	0.15	7.84	10.95	3.11	0.34

To better understand the influences of the introduced MoS_2 on the transmission spectra and the physical process involved, we have performed the simulation of the surface currents and electric field distributions of SRR/SiO_2 structure without and with MoS_2 overlayer, as shown in Figs. 2(c) and 2(d), respectively. It can be observed LFRM stems from LC resonance with a circular current and its electric field is highly concentrated around the gap. HFRM primarily arises from the dipole resonance with linear current and its electric field is mainly distributed at the gap and both ends of the bottom edge. The surface current intensities as well as the electric field intensities all decrease after covering the overlayer. It is known that the resonant frequency of LFRM can be defined as $1/2\pi\sqrt{LC}$, where the inductance L is mainly determined by the geometry of SRR and the capacitance C is highly relevant to both the gap dimension and the surrounding medium.[28] With the introduction of MoS_2, the average permitivity of hybrid sample is increased to enhance the total capacitance, resulting in the red-shift of LFRM. That means this red-shift depends on the dielectric property of the overlayer near the gap of SRR. Furthermore, MoS_2 could make the positive and negative charges neutralize near the gap to reduce the currents intensity and the resonant electric field, which causes the increased transmission of LFRM in MoS_2 hybrid structure. HFRM as a plasmonic dipole can be approximately described with the resonant frequency of $1/\left(4\pi d\sqrt{\varepsilon_{\mathrm{ave}}}\right)$,[22,35] where d is the arm length and $\varepsilon_{\mathrm{ave}}$ is the average dielectric constant of surrounding medium. Similarly, the $\varepsilon_{\mathrm{ave}}$ will increase after covering MoS_2 layer, leading to the red shift of resonance frequency.[36] Importantly, under the influence of THz electric field, MoS_2 dielectric layer will be polarized accompanied with the generation of polarized charges, which could induce the depolarization field and weaken the original applied electric field. The depolarization field will restrict the electrons' movement in SRRs driven by the incident THz wave.[37,38] Then the resonant electric field intensities at HFRM are largely reduced, leading to the weakening of dipole resonance to enhance the THz transmission at resonant mode.

3. Tunable transmission behaviors

Since the introduction of MoS_2 can significantly modify the transmitted behaviors, it provides us a pathway to actively tune the spectra to achieve THz modulator and optical switch devices via controlling the overlayer conductivity. Hence, we have simulated the THz transmission response of MoS_2/SRR/SiO_2 structure with different electrical conductivities of MoS_2 overlayer, as indicated in Fig. 3. The spectra exhibit the redshift in frequency and decreased resonant response when the electrical conductivity is increased to 1200 S/m, as depicted in Fig. 3(a). Here, we define the relevant parameters ΔT_{non}, $\Delta T^{\mathrm{off}}_{\mathrm{LFRM}}$, and $\Delta T^{\mathrm{on}}_{\mathrm{LFRM}}$. ΔT_{non} indicates the transmission variation in off-resonant region corresponding to the absorption of THz wave response A_{non}. $\Delta T^{\mathrm{off}}_{\mathrm{LFRM}}$ and $\Delta T^{\mathrm{on}}_{\mathrm{LFRM}}$ represent the depths of the resonant lineshapes related to A_{LFRM} at LFRM with zero and non-zero conductivities of MoS_2 overlayer, respectively. For the HFRM, the definition is similar. It is extracted that the A_{LFRM}, A_{HFRM}, and A_{non} are 0.09, 0.30,

and 0.19, respectively under the conductivity of 1200 S/m. In addition, we have presented more detailed spectral change in the conductivity range of 100 S/m to 3800 S/m, as plotted in Fig. 3(b). For the resonant region, the LFRM can be quenched when the conductivity is further increased to 3500 S/m, while the HFRM still remains a weak resonance. This suggests the LC mode of LFRM is more sensitive to the surface permittivity surrounding, leading to a switch effect in resonance. For the off-resonant region, the transmission gradually decreases and the corresponding absorption increases 38% in the broad range from 0.95 THz to 1.95 THz, seen from black shadow area in Fig. 3(b), showing that an option for controllable THz modulator in a wide bandwidth could be realized. It is also worth noting that the significant transmission difference in resonant and off-resonant regions has strong correlation with the overlayer conductivity, namely the varied conductivity of MoS_2 overlayer is responsible for the changes in THz response. To further figure out the appeared switch effect in the hybrid MoS_2/SRR structure, figures 3(c) and 3(d) exhibit the numerically calculated simulated electric field distributions in the hybrid structure at the LFRM and HFRM with the tuned MoS_2 conductivity of 0, 300, 1200, and 3500 S/m, respectively. The results show the increased conductivity of MoS_2 layer leads to the decreased electric field in the capacitance gap as well as the reduced electric field around the arm in SRR structure, which eventually causes the weakening of HFRM and quenching of LFRM. The annihilation of electric field at higher conductivity implies the switching-off of the LFRM in the hybrid metamaterial system.

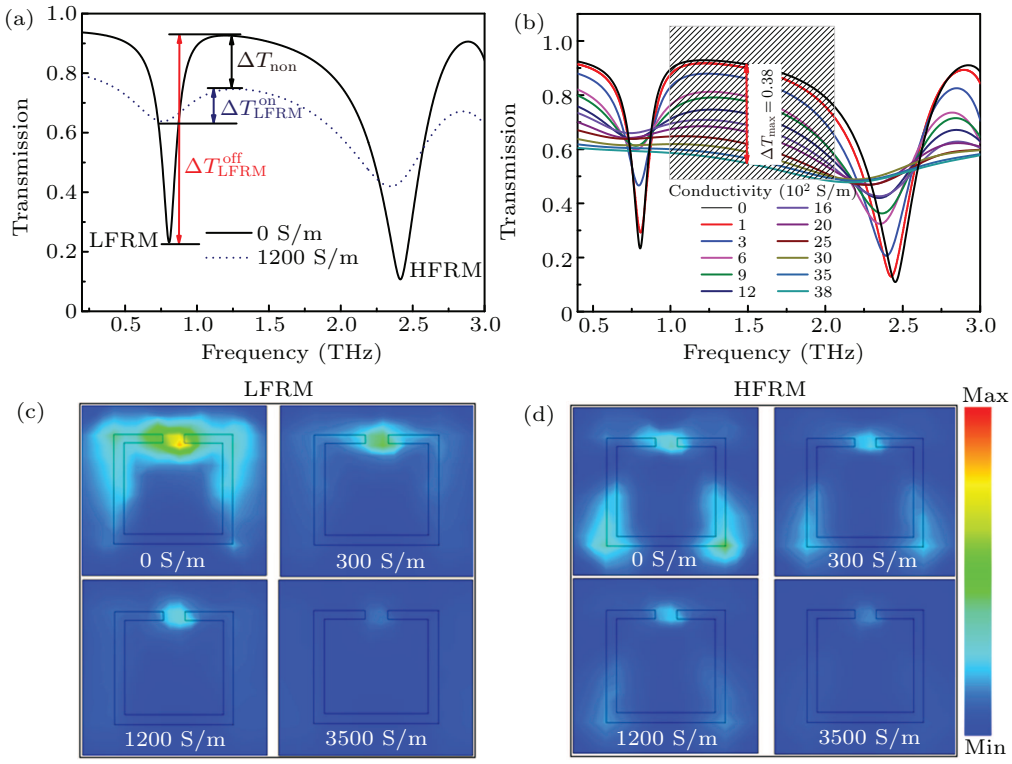


Fig. 3. (a) and (b) Simulated amplitude transmission spectra with different electrical conductivities of MoS_2 overlayer and the definition of the parameters of ΔT_{non}, ΔT^{off}_{LFRM}, and ΔT^{on}_{LFRM}. (c) and (d) Simulated electric field distributions in the hybrid metamaterial at LFRM and HFRM, respectively.

Then we have extracted the conductivity-dependent absorption of THz wave responses to explore the quantitive relation between spectral evolution and the tunable MoS_2 overlayer. It can be seen that A_{LFRM} and A_{HFRM} can be expressed by the decreased exponential fittings, as given in Fig. 4(a). The curve of LFRM reaches zero faster than that of HFRM, also implying that the LC resonance is more susceptible to the overlayer conductivity than the dipole resonance. However, A_{non} can be well fitted by an exponential growth function, showing the remarkable absorption of THz wave enhancement in off-resonant region with the increased conductivity of MoS_2 overlayer. Meanwhile, the dependency between the resonant frequency shift and the overlayer electrical conductivity is plotted in Fig. 4(b) for LFRM and HFRM, respectively, showing monotonic increasing linear relationships with much larger frequency shift at HFRM. The resonant linewidth changes linearly as well, as presented in Fig. 4(c). It is indicated that the lineshape is significantly tuned with the conductivity of surface layer. Hence, we further analyze and study the active modulation performance of MoS_2/SRR/SiO_2 structure. We define the peak to dip transmission amplitude modulation depth of LFRM as $\left[\left(\Delta T^{off}_{LFRM} - \Delta T^{on}_{LFRM}\right)/\Delta T^{off}_{LFRM}\right] \times 100\%$, as shown in Fig. 4(d).

The modulation depth of HFRM is similar. We have

found that the modulation depth can be tuned to 90% at HFRM. For LFRM, this modulation is much higher and can achieve 100% by increasing the conductivity to 3500 S/m, which infers the occurrence of a switchable resonant behaviour. This effect could serve as a tunable MoS_2-based switch device when the conductivity of MoS_2 is tuned under the external field. It is evident that the tunable THz behaviors strongly depend on the properties of MoS_2 layer. Hence, we further discuss the influence of its thickness on the amplitude transmission. Our simulated results exhibit the remarkable red-shift of LFRM and HFRM with the increased thickness. The resonant intensity is reduced slightly at LFRM and nearly unchanged at HFRM. Additionally, the bandwidth of the off-resonant region has a narrowing trend (not shown).

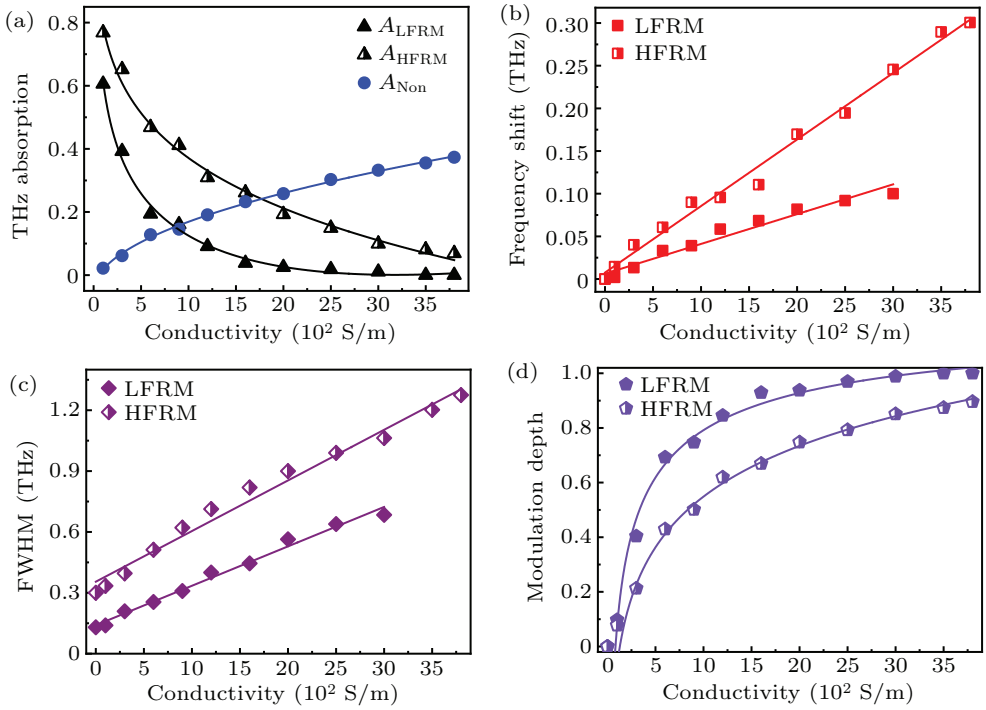


Fig. 4. (a) Extracted THz absorption response of the hybrid structure with different overlayer conductivities. Influence of the overlayer conductivity on the resonant frequency shift (b), bandwidth of resonant regions (c), and modulation depth (d) for LFRM and HFRM, respectively. The solid lines are the fitting curves.

4. Theoretical coupling mechanism

For better understanding these phenomena and explaining the coupling mechanism in the hybrid metamaterial, a Lorentz coupling model[35,36,39] is used to explain the variations in transmission spectra and quantitatively reveal the interaction between MoS_2 and SRR in THz region. This coupling model can be expressed as

$$\ddot{x}_1 + \gamma_1 \dot{x}_1 + \omega_1^2 x_1 + \upsilon_{12} x_2 = a_1 \mathrm{e}^{\mathrm{i}\omega t}, \tag{1}$$

$$\ddot{x}_2 + \gamma_2 \dot{x}_2 + \omega_2^2 x_2 + \upsilon_{12} x_1 = a_2 \mathrm{e}^{\mathrm{i}\omega t}, \tag{2}$$

where x_1, x_2, γ_1, γ_2, ω_1, ω_2 are the amplitudes, damping rates, and resonance frequencies for the metamaterial and MoS_2 overlayer, respectively. υ_{12} represents the coupling coefficient between their resonances. The geometric parameters a_1 and a_2 indicate the strength of each material coupling to the incident THz field. Here, we consider the steady-state solutions for the displacement of the oscillators are $x_1 = C_1 \mathrm{e}^{\mathrm{i}\omega t}$ and $x_2 = C_2 \mathrm{e}^{\mathrm{i}\omega t}$. The amplitude of first oscillator has the form

$$C_1 = \frac{a_1\left(\omega_2^2 - \omega^2 + \mathrm{i}\gamma_2\omega\right) - a_{12}\upsilon_{12}}{\left(\omega_1^2 - \omega^2 + \mathrm{i}\gamma_1\omega\right)\left(\omega_2^2 - \omega^2 + \mathrm{i}\gamma_2\omega\right) - \upsilon_{12}^2}. \tag{3}$$

Then the THz response intensity of metamaterial without and with the MoS_2 overlayer can be obtained by plotting the curve of $|C_1|$, as depicted in Figs. 5(a) and 5(b) under the initial values of $\gamma_1 = 0.025$, $\omega_1 = 1.0$, $a_1 = 2.0$, $\gamma_2 = 0.01$, $\omega_2 = 1.3$, $a_2 = 1.1$, and $\upsilon_{12} = 0.5$. Notably, the variation of THz response intensity in resonant region is consistent with the simulated observation of THz transmission of SRR structure without and with MoS_2 overlayer illustrated in Fig. 2(b), showing a red-shift accompanied with the reduction in resonant absorption and broadening in bandwidth. To understand the influence of the coupling and damping of MoS_2 on metamaterials, we further modify the parameters υ_{12} and γ_2, as shown in Figs. 5(c) and 5(d), respectively, while keeping other parameters constant. It is evident that υ_{12} determines both frequency shift and the intensity of the resonance, showing the stronger coupling leads to the larger red-shift and lower peak intensity. Damping rate γ_2 as an important parameter mainly affects the shape as well as the bandwidth of the resonance with the higher damping for broader spectral response.

In Fig. 6(a), further calculations suggest that the THz response peak intensity is exponential decay with the υ_{12} (black triangles). However, the THz intensity in off-resonant region

is exponential growth with the υ_{12} (blue dots). The red squares and its fitting curve show the linear dependency between the red-shift frequency and coupling strength. Similar to the influence of υ_{12}, the THz response intensity in the resonant region also exhibits exponential decay with γ_2, as shown in Fig. 6(b). In addition, the linear increasing of resonant bandwidth with γ_2 is illustrated by FWHM. It is worth highlighting that the above observed tendency agrees well with the simulated results depicted in Fig. 4, implying a stronger coupling effect with higher υ_{12} will occur in the hybrid structure with the increased electrical conductivity. Moreover, this effect will result in large frequency red-shift and transmission change in THz resonant and off-resonant regions. The identical linear increasing of FWHM with overlayer conductivity in Fig. 4(c) and with the damping rate in Fig. 6(b) suggests that γ_2 is highly related to the conductivity of MoS_2 overlayer, which means the THz transmission loss of MoS_2 coating layer will increase with increasing conductivity. The obtained results could help to further reveal the interaction between MoS_2 and metamaterials.

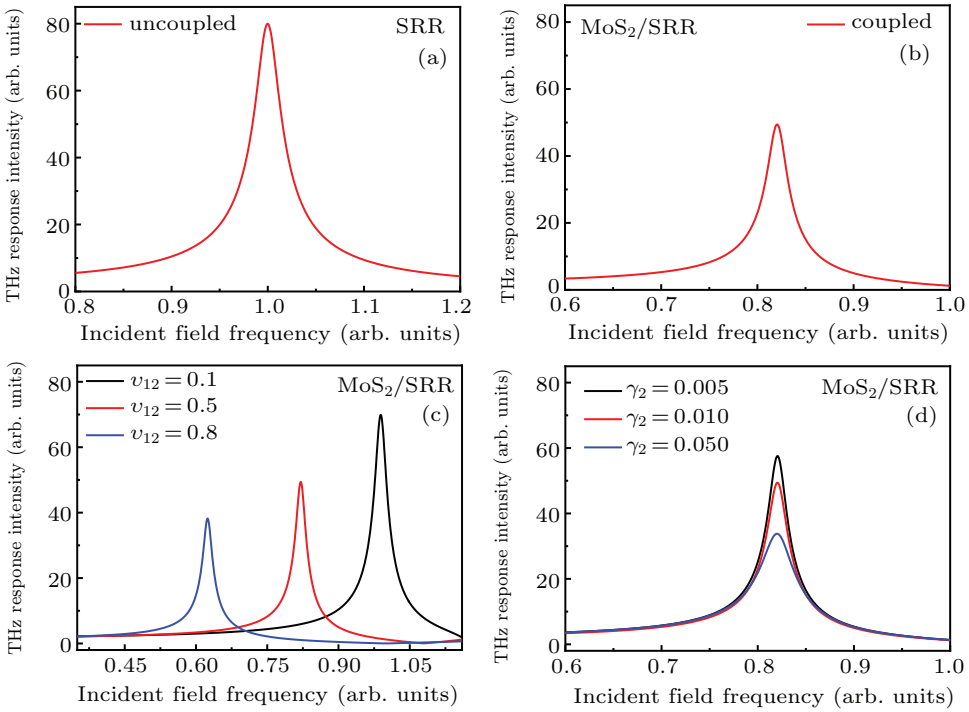


Fig. 5. Panels (a) and (b) are the THz response intensity of the uncoupled SRR and coupled MoS_2/SRR system. Panels (c) and (d) are the THz response intensity of MoS_2/SRR system under the different coupling coefficients υ_{12} and damping rates γ_2, while keeping other parameters constant.

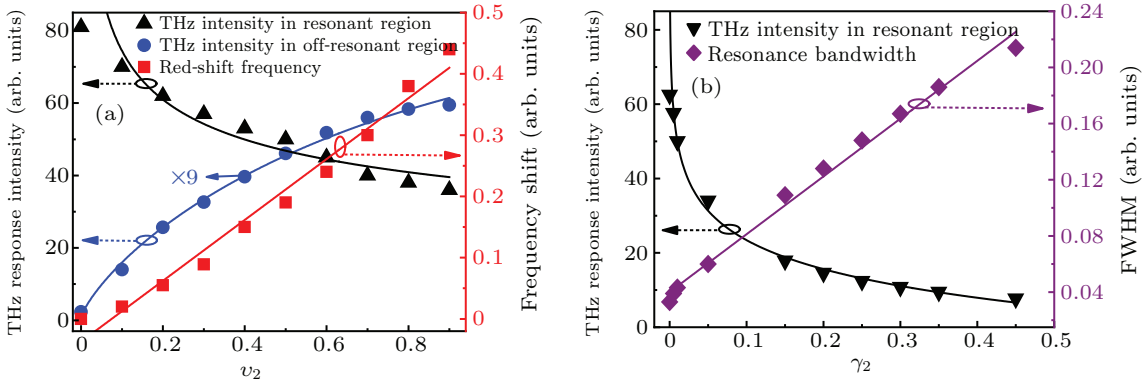


Fig. 6. (a) Influence of υ_{12} on THz response intensity in resonant region (black triangles) and off-resonant region (blue dots). The curves are the exponential fitting. Influence of υ_{12} on frequency red-shift (red squares). The curve is the linear fitting. (b) Influence of γ_2 on THz response intensity and bandwidth.

5. Conclusion

In summary, we propose a hybrid structure composed of MoS_2 layer and SRR arrays on different substrates to efficiently control THz wave. The simulated results indicate that the hybrid MoS_2/SRR/SiO_2 is more susceptible to THz field, showing large frequency red-shift and bandwidth broadening. Our studies also elucidate that the top cover MoS_2layer with varied conductivity could distinctly manipulate the THz response. Specifically, this hybrid structure can realize a 38% wide-band modulator in off-resonant region, 90% modulation

of dipole resonance, and 100% modulation depth of LC resonance with a switch effect. In addition, a Lorentz coupling model is employed to theoretically investigate the influence of MoS_2 on the THz response spectra and the coupling interaction between MoS_2 overlayer and SRR structure. We find the characteristics of conductivity-induced changes in transmission spectra with frequency red-shift, bandwidth broadening, and variation of THz response intensity mainly originate from the coupling and damping between MoS_2 overlayer and the SRR arrays. Our work will provide an option for tunable THz modulators, switchable devices and other THz functional components for THz wave manipulation based on MoS_2 material.

Acknowledgements

Project supported by Beijing Natural Science Foundation of China (Grant No. 4181001) and the National Natural Science Foundation of China (Grant Nos. 62075142 and 61875140).

References

[1] Ganatra R and Zhang Q 2014 *ACS Nano* **8** 4074
[2] Dankert A and Dash S P 2017 *Nat. Commun.* **8** 16093
[3] Rukelj Z, Strkalj A and Despoja V 2016 *Phys. Rev. B* **94** 115428
[4] Huang Y L, Chen Y, Zhang W, Quek S Y, Chen C H, Li L J, Hsu W T, Chang W H, Zheng Y J, Chen W and Wee A T 2015 *Nat. Commun.* **6** 6298
[5] Mak K F, Lee C, Hone J, Shan J and Heinz T F 2010 *Phys. Rev. Lett.* **105** 136805
[6] Radisavljevic B, Radenovic A, Brivio J, Giacometti V and Kis A 2010 *Nat. Nanotechnol.* **6** 147
[7] Jariwala D, Sangwan V K, Lauhon L J, Marks T J and Hersam M C 2014 *ACS Nano* **8** 1102
[8] Lopez-Sanchez O, Lembke D, Kayci M, Radenovic A and Kis A 2013 *Nat. Nanotechnol.* **8** 497
[9] Srivastava Y K, Chaturvedi A, Manjappa M, Kumar A, Dayal G, Kloc C and Singh R 2017 *Adv. Opt. Mater.* **5** 1700762
[10] Splendiani A, Sun L, Zhang Y, Li T, Kim J, Chim C Y, Galli G and Wang F 2010 *Nano Lett.* **10** 1271
[11] Yin Z, Li H, Jiang L, Shi Y, Sun Y, Lu G, Zhang Q, Chen X and Zhang H 2012 *ACS Nano* **6** 74
[12] Mouri S, Miyauchi Y and Matsuda K 2013 *Nano Lett.* **13** 5944
[13] Amani M, Lien D H, Kiriya D, Xiao J, Azcatl A, Noh J, Madhvapathy S R, Addou R, KC S, Dubey M, Cho K, Wallace R M, Lee S C, He J H, Ager J W, Zhang X, Yablonovitch E and Javey A 2015 *Science* **350** 1065
[14] Mak K F, McGill K L, Park J and McEuen P L 2014 *Science* **344** 1489
[15] Geim A K and Grigorieva I V 2103 *Nature* **499** 419
[16] Fang H, Battaglia C, Carraro C, Nemsak S, Ozdol B, Kang J S, Bechtel H A, Desai H, Kronast F, Unal A A, Conti G, Conlon C, Palsson G K, Martin M C, Minor A M, Fadley C S, Yablonovitch E, Maboudian R and Javey A 2014 *Proc. Natl. Acad. Sci. USA* **111** 6198
[17] Arnold A J, Razavieh A, Nasr J R, Schulman D S, Eichfeld C M and Das S 2017 *ACS Nano* **11** 3110
[18] Veselago V G 1968 *Sov. Phys. Usp.* **10** 509
[19] Smith D R, Padilla W J, Vier D C, Nemat-Nasser S C and Schultz S 2000 *Phys. Rev. Lett.* **84** 4184
[20] Fang N, Lee H, Sun C and Zhang X 2005 *Science* **308** 534
[21] Shalaev V M 2007 *Nat. Photon.* **1** 41
[22] Pendry J B, Holden A, Robbins D and Stewart W 1999 *IEEE Trans. Microwave Theory Tech.* **47** 2075
[23] Schurig D, Mock J J, Justice B J, Cummer S A, Pendry J B, Starr A F and Smith D R 2006 *Science* **314** 977
[24] Soukoulis C M, Kafesaki M and Economou E N 2006 *Adv. Mater.* **18** 1941
[25] Soukoulis C M, Linden S and Wegener M 2007 *Science* **315** 47
[26] Deng Y W, Zhou Q L, Zhang P J, Jiang N, Ning T, Liang W L and Zhang C L 2021 *ACS Appl. Mater. Interfaces* **13** 13565
[27] Ji J, Zhou S, Wang W, Ling F and Yao J 2019 *Nanoscale* **11** 9429
[28] Padilla W J, Taylor A J, Highstrete C, Lee M and Averitt R D 2006 *Phys. Rev. Lett.* **96** 107401
[29] Li C, Zhou Q L, Shi Y L, Yang Z, Shi L and Zhang C L 2017 *Opt. Commun.* **391** 77
[30] Kim T T, Kim H D, Zhao R, Oh S S, Ha T, Chung D S, Lee Y H, Min B and Zhang S 2018 *ACS Photonics* **5** 1800
[31] Hu Y, You J, Tong M, Zheng X, Xu Z, Cheng X and Jiang T 2020 *Adv. Sci.* **7** 2000799
[32] Hu Y, Jiang T, Sun H, Tong M, You J, Zheng X, Xu Z and Cheng X 2020 *Laser Photon. Rev.* **14** 1900338
[33] Zhou J, Zhang C, Liu Q, You J, Zheng X, Cheng X and Jiang T 2020 *Nanophotonics* **9** 2797
[34] Wu J Y, Xu X F and Wei L F 2020 *Chin. Phys. B* **29** 094202
[35] Li J, Zhou Y, Quan B, Pan X, Xu X, Ren Z, Hu F, Fan H, Qi M, Bai J, Wang L, Li J and Gu C 2014 *Carbon* **78** 102
[36] Su X, Ouyang C, Xu N, Tan S, Gu J, Tian Z, Singh R, Zhang S, Yan F, Han J and Zhang W 2015 *Sci. Rep.* **5** 10823
[37] Alloway D M, Hofmann M, Smith D L, Gruhn N E, Graham A L, Colorado R, Wysocki V H, Lee T R, Lee P A and Armstrong N R 2003 *J. Phys. Chem. B* **107** 11690
[38] Sun Y, Xia X, Feng H, Yang H, Gu C and Wang L 2008 *Appl. Phys. Lett.* **92** 221101
[39] Wang Q, Huang Y, Yao Z and Xu X 2016 *Opt. Quantum Electron.* **48** 83